Acoustic Bound Pairs under Nonreciprocal Two-Body Interactions

Zhenhang Pu,[1] Yuxiang Xi,[1] Yugan Tang,[2] Jiuyang Lu,[1] Weiyin Deng,[1,*] Hua Cheng,[2] Manzhu Ke,[1,†] Shuqi Chen,[2] and Zhengyou Liu[1,3,‡]

[1]*Key Laboratory of Artificial Micro- and Nanostructures of Ministry of Education and School of Physics and Technology, Wuhan University, Wuhan 430072, China*

[2]*The Key Laboratory of Weak Light Nonlinear Photonics, Ministry of Education, School of Physics and TEDA Institute of Applied Physics, Nankai University, Tianjin 300071, China*

[3]*Institute for Advanced Studies, Wuhan University, Wuhan 430072, China*

(Received 9 December 2025; revised 27 January 2026; accepted 11 March 2026; published 7 April 2026)

The exploration of many-body problems stands at the vanguard of modern physics, presenting profound challenges alongside compelling opportunities. Recently, the non-Hermiticity featured with complex spectra has significantly expanded the landscape of many-body phenomena beyond the Hermitian paradigm. Most existing studies focus on the interplay between non-Hermiticity and many-body interactions, with the latter being Hermitian in isolation. Here, by integrating nonreciprocity, a key mechanism inducing non-Hermiticity, into two-body interactions, we analytically demonstrate how such interactions govern correlated pair and experimentally confirm our prediction in a phononic crystal simulator. Resulting phenomena, including the non-Hermitian inverse skin effect where the particles undergo synchronous motion as a bound pair and accumulate opposite to the dominant hopping direction, as well as the time cluster effect where two initially separate particles tend to cluster and last as a bound pair in the time domain, are unambiguously captured in airborne sound measurements. These findings experimentally unveil the unique phenomena driven by nonreciprocal many-body interactions, opening new pathways for controlled engineering in correlated systems.

DOI: 10.1103/xr3h-j9pv

The exploration of physical phenomena in strongly correlated systems has emerged as one of the most challenging yet fascinating frontiers in modern physics [1]. The many-body interactions, such as electron-electron interaction and magnetic exchange interaction, play essential roles in fostering novel quantum phases, including the fractional quantum Hall effect [2,3] and the quantum spin liquids [4,5]. Serving as fundamental building blocks for understanding many-body phenomena, few-body problems have attracted considerable attention throughout recent decades owing to the significant experimental advances in ultracold atomic systems [6–11]. Unlike quantum systems, classical wave systems such as photonic crystals for electromagnetic waves and phononic crystals (PCs) for acoustic waves, naturally lack many-body interactions. However, by mapping the dynamics of correlated particles onto a single particle in higher dimensions [12], implementation and precisely control of few-body interactions (especially of two- and three-body interactions) become accessible for classical waves. For instance, the fractional Bloch oscillations [13,14] in photonic waveguides, and topological edge states induced by interacting bound pairs [15,16] and anyonic statistics [17,18] in electric circuits are implemented. Despite these advances, many-body physics remains unexplored in PCs for acoustic waves to date.

Non-Hermitian physics, featured with complex energy spectra, has established itself as a transformative framework for controlling open systems in the presence of nonreciprocity, gain, and loss, and extends quantum mechanics beyond the Hermitian paradigm [19–21]. Because of the spectral topology, non-Hermitian systems exhibit numerous intriguing phenomena including the exceptional points and non-Hermitian skin effects (NHSEs). A canonical example for NHSEs is the Hatano-Nelson model [22], a one-dimensional (1D) chain with nonreciprocal hoppings, where all the eigenstates accumulate along the dominant hopping direction and localize at open boundary as skin modes. While the majority of current studies concentrates on single-body systems, research interest in non-Hermitian many-body problems is witnessing explosive growth, catalyzing seminal works such as dissipation-induced correlations [23], skin clusters [24–26], and bound states in the continuum [27]. Among them, given the pivotal role of nonreciprocity in exploring non-Hermitian physics, many-body interactions are typically introduced to lattices with nonreciprocal hoppings to probe their interplay or competition. Inspired by the intriguing non-Hermitian

*Contact author: dengwy@whu.edu.cn
†Contact author: mzke@whu.edu.cn
‡Contact author: zyliu@whu.edu.cn

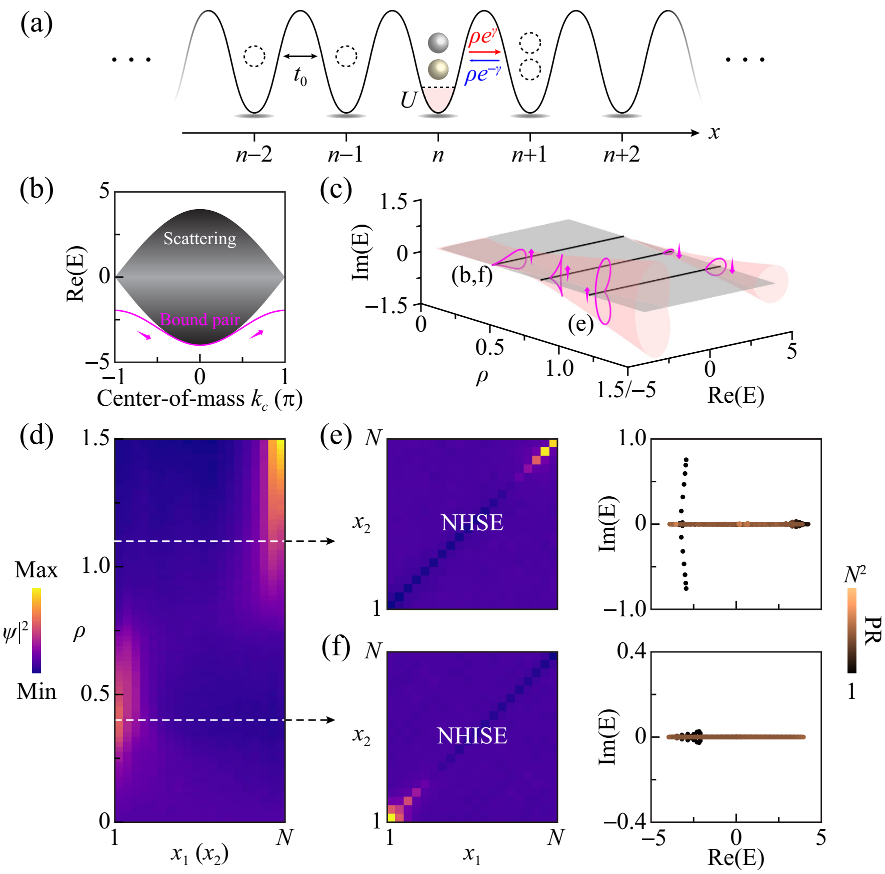

FIG. 1. Correlated particles under nonreciprocal two-body interaction. (a) Schematics of a 1D lattice possessing two bosons. Non-Hermiticity is introduced by the nonreciprocal two-body hoppings $\rho e^{\pm\gamma}$. (b) Real part of the PBC energy spectrum, as a function of center-of-mass momentum k_c. The shaded continuum and the magenta line correspond to scattering states and bound pair states, respectively. (c) Complex PBC energy spectrum under different two-body hopping strength ρ. (d) Spatial distribution of one particle under OBC when varying ρ. (e) A NHSE where the two particles behave as a bound pair and accumulate along the dominant hopping direction. Left panel: two-body wave function for all eigenstates (modulus square). Right panel: complex energy spectrum. The color map gives the PR. (f) A NHISE where the collapse direction is opposite to the dominant hopping direction. The parameters are chosen as $N = 20$, $t_0 = -1$, $U = -1$, $\gamma = 0.6$, $\rho = 0.4$ (b),(f) and 1.1 (e).

properties under the simplest single-body nonreciprocal hopping in the Hatano-Nelson model, a fundamental question is raised: what will happen when many-body interaction is nonreciprocal?

Here we theoretically propose a modified Bose-Hubbard model with nonreciprocal two-body interactions and experimentally investigate the non-Hermitian dynamics of corrected pairs using a PC simulator. With each dimension describing the position of one particle, the PC sample is implemented in two dimensions to simulate two bosons moving on a 1D lattice. The nonreciprocal two-body interaction is mapped to the unidirectional acoustic couplings along the PC diagonal, achieved via a set of active electroacoustic couplers (AECs) [28–31]. The nearest-neighbor two-body hoppings can trigger a non-Hermitian inverse skin effect (NHISE), where the particles undergo synchronous motion as a bound pair and accumulate opposite to the dominant hopping direction. More interestingly, the system exhibits a time cluster effect, where two initially separated particles tend to cluster and eventually remain as a bound pair in the time domain, even under the onsite two-body repulsive interactions that typically isolate particles. Our findings, employing PC as a classical-wave simulator to investigate non-Hermitian many-body physics, unveil the unique phenomena driven by nonreciprocal many-body interactions.

Nonreciprocal two-body interaction and NHISE—We propose a non-Hermitian Bose-Hubbard model with nonreciprocal two-body interaction, which possesses two correlated spinless bosons. The corresponding 1D lattice is illustrated in Fig. 1(a). The Hamiltonian is

$$H = t_0 \sum_n \left(\hat{a}_n^\dagger \hat{a}_{n+1} + \hat{a}_{n+1}^\dagger \hat{a}_n \right) + \frac{U}{2} \sum_n \hat{a}_n^\dagger \hat{a}_n^\dagger \hat{a}_n \hat{a}_n + \frac{\rho e^{-\gamma}}{2} \sum_n \hat{a}_n^\dagger \hat{a}_n^\dagger \hat{a}_{n+1} \hat{a}_{n+1} + \frac{\rho e^{\gamma}}{2} \sum_n \hat{a}_{n+1}^\dagger \hat{a}_{n+1}^\dagger \hat{a}_n \hat{a}_n. \quad (1)$$

Here, $\hat{a}_n(\hat{a}_n^\dagger)$ is the annihilation (creation) operator for the boson at site n (of N total sites). t_0 is the single-body hopping strength, and U describes the onsite two-body interactions (attractive for $U < 0$ and repulsive for $U > 0$). Non-Hermiticity is solely brought by the nearest-neighbor nonreciprocal two-body hoppings $\rho e^{\pm\gamma}$ $(\gamma > 0)$, denoted by the red and blue arrows. This feature distinguishes our system from previous works where the nonreciprocal hoppings and the many-body interactions are typically introduced separately.

The two-body state vector can be expanded in Fock space as $|\psi\rangle = (1/\sqrt{2})\sum_{x_1,x_2} u(x_1,x_2)\hat{a}_{x_1}^\dagger\hat{a}_{x_2}^\dagger|0\rangle$, where $|0\rangle$ is the vacuum state and $u(x_1,x_2)$ is the probability amplitude with one particle at site x_1 and the other at site x_2. Introducing center-of-mass and relative coordinates $c = [(x_1+x_2)/2]$ and $r = x_1 - x_2$, the energy spectrum under periodic boundary condition (PBC) can be solved; see derivation in Supplemental Material [32]. Figure 1(b) displays the band structure as a function of center-of-mass momentum k_c, including two types of states: the shaded continuum corresponds to scattering states that the particles are far apart and move independently on the lattice; the magenta line represents bound pair states that the particles appear at the same site and move together. These bands are also depicted in the complex plane in Fig. 1(c). Three slices of the spectra under typical ρ are highlighted by solid lines, and the left slice corresponds to Fig. 1(b). Since the non-Hermiticity arises exclusively from interaction terms, the scattering states (black) are confined to the real axis. In contrast, the bound pair states (magenta) possess complex energies and wind in the complex plane as k_c goes (along the magenta arrows). The spectral topology of such anticlockwise band winding is characterized by a positive winding number $v = 1$. When increasing ρ, besides the emergence of the second bound pair band with a larger real part, the first band undergoes a progressive twist and eventually reverses its winding orientation (from anticlockwise to clockwise winding), which corresponds to a negative $v = -1$. In single-body problems, a nonzero v implies the existence of NHSE under open boundary condition (OBC), and, according to the non-Bloch band theory [34–38], the sign of v determines the collapse direction of skin modes. In other words, the orientation reversal of band winding leads to a reversal of collapse direction of skin modes. This motivates our subsequent verification of whether such correspondence between spectral topology and NHSE holds universally in our correlated system.

To this end, we proceed to investigate the localization feature of OBC eigenstates, as presented in Fig. 1(d). For a fixed ρ, the color map is given by $\sum_{n,x_2}|u_n(x_1,x_2)|^2$, denoting the spatial distribution of one particle. Results for the two particles are the same owing to the exchange symmetry of bosons $u_n(x_1,x_2) = u_n(x_2,x_1)$. For smaller ρ, the particle tends to accumulate along the $-x$ direction and localize the left boundary, which reveals as the counterintuitive NHISE since the rightward two-body hopping is much stronger than the leftward one. When ρ exceeds a threshold at around 0.8, the collapse direction reverses and aligns with the $+x$ direction, corresponding to the conventional NHSE. Figures 1(e) and 1(f) exemplify two typical cases for NHSE and NHISE, respectively, with $\rho = 1.1$ and 0.4 as taken in the right and left slices in Fig. 1(c). The left panels display the two-body wavefunctions, where the bright spots along the diagonal line $x_1 = x_2$ reflect the synchronous localization of the particles as bound pairs. The right panels represent the OBC spectra, and the colormaps denote the participation ratio defined as $\mathrm{PR} = (\sum_{x_1,x_2}|u_n(x_1,x_2)|^2)^2/\sum_{x_1,x_2}|u_n(x_1,x_2)|^4$. This confirms that the occurrence of NHSE and NHISE is determined by the center-of-mass band winding [32].

Time evolution—We then investigate the motion of correlated particles in the time domain. Based on the system parameters in Fig. 1(e), a two-body initial state $|\psi_0\rangle$ is prepared with its wavefunction taken the Gaussian form as $u_0(x_1,x_2) = Ae^{-(x_1-m_0)^2-(x_2-n_0)^2}$. Here, A is the normalization factor, m_0 and n_0 represent the coordinates of two initially separated particles, which are randomly chosen as $(m_0,n_0) = (17,6)$ of $N = 20$ total sites. Figure 2(a) displays the evolution of the particles in the

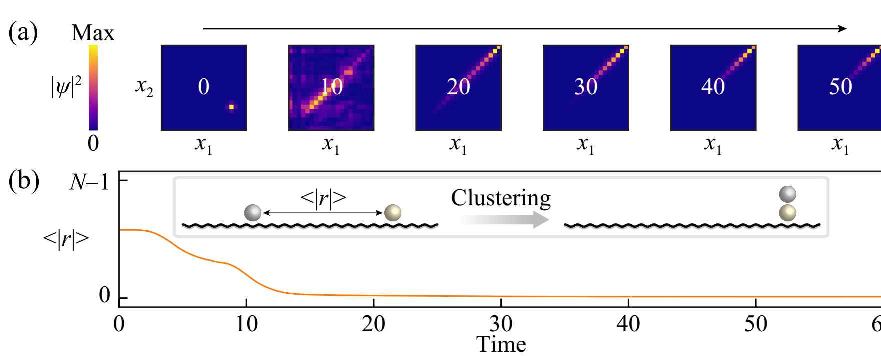

FIG. 2. Time evolution of two initially separated particles. (a) Snapshots of the two-body wavefunction at discretized times, with respect to two initially separated particles. (b) Time evolution of the expected value $\langle|r|\rangle$. The inset illustrates the time cluster effect. The lattice parameters are the same as Fig. 1(e).

time domain with a step of 10. The colormaps give the distributions of final states $|\psi(t)\rangle = A(t)e^{-iHt}|\psi_0\rangle$, which are individually normalized for better visualization. The reduced Planck constant $\hbar$ is omitted. It is shown that, after a dynamical evolution of time, the wave function soon distribute along the diagonal line, implying the clustering of particles, namely, the time cluster effect. Driven by the NHSE, the particles move as a bound pair towards the open boundary and eventually remain stable.

To further demonstrate the time cluster effect, we display the time evolution of $\langle|r|\rangle$ in Fig. 2(b). The expected value $\langle|r|\rangle = \langle\psi(t)||\hat{r}||\psi(t)\rangle$ denotes the average distance between the particles, and naturally, as depicted by the orange curve, equals to $|m_0 - n_0| = 9$ for the initially separated particles at time $t = 0$. When undergoing the particle clustering, $\langle|r|\rangle$ approaches zero asymptotically with increased time. The above process is schematically illustrated by the inset. In essence, the time cluster effect originates from the skin mode with the largest imaginary part [in the right panel of Fig. 1(e)], which dominates the final state as a bound pair in the long-time limit, regardless of the initial position of the particles. As the imaginary parts of eigenenergies (specifically non-Hermiticity) are solely induced by the nonreciprocal two-body hoppings, the occurrence of the time cluster effect is insensitive to other parameters including the onsite two-body interaction. As an intriguing result, this effect can counterintuitively occur in the presence of repulsive interactions, which typically isolate the particles [32].

Non-Hermitian acoustic bound pairs—Next, we map the aforementioned two-body dynamics onto the propagation of scalar acoustic waves in a 2D PC. Derived from the Schrödinger equation $H|\psi\rangle = E|\psi\rangle$ for the Hamiltonian in Eq. (1), the eigenequation with respect to $u(x_1, x_2)$ reads

$$\begin{aligned} Eu(x_1,x_2) = t_0[&u(x_1-1,x_2)+u(x_1,x_2-1)\\ &+u(x_1+1,x_2)+u(x_1,x_2+1)]\\ &+\delta_{x_1,x_2}[Uu(x_1,x_2)+\rho e^{-\gamma}u(x_1+1,x_2+1)\\ &+\rho e^{\gamma}u(x_1-1,x_2-1)], \end{aligned} \tag{2}$$

which can also be viewed as the equation of a single particle moving on the 2D lattice in Fig. 3(a). With each dimension describing the position of one boson ($x_{1,2}$), the 2D lattice consists of $N \times N$ sites (spheres) and each corresponds to a two-body basis $(1/\sqrt{2})\hat{a}^\dagger_{x_1}\hat{a}^\dagger_{x_2}|0\rangle$. The center-of-mass and relative coordinates are labeled by the 45°-tilted c-r axes. Note that, as both x_1 and x_2 vary from 1 to N, $c = [(x_1 + x_2)/2]$ varies from 1 to N while $r = x_1 - x_2$ varies from $1 - N$ to $N - 1$. In parallel, the single-body hoppings t_0 are mapped to the horizontal and vertical hoppings (black sticks), and the onsite two-body interaction U is

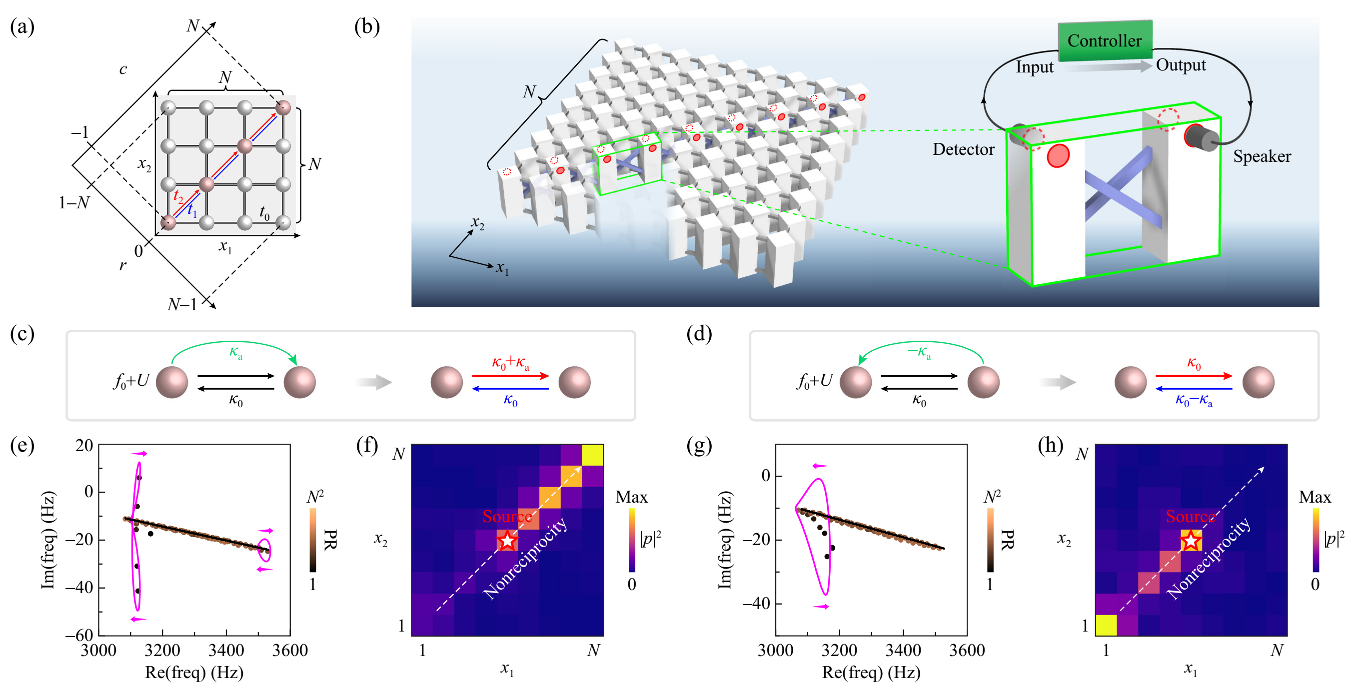

FIG. 3. Demonstration of non-Hermitian acoustic bound pairs. (a) Mapping 1D correlated system onto a 2D lattice. The nonreciprocal two-body hoppings are embodied in the hoppings between diagonal sites. (b) Acoustic realization of the lattice model. Left panel: schematics of the PC. Right panel: magnified view of the acoustic nonreciprocal hopping. (c),(d) Schematics of two AEC setups with larger (c) and smaller (d) nonreciprocal hopping strengths. (e) Retrieved complex frequency spectrum of the PC with the setup in (c). (f) Observation of the NHSE of acoustic bound pairs. The color map represents measured acoustic signals (modulus square). (g),(h) The same as (e) and (f), but adopting the setup in (d) to observe the NHISE.

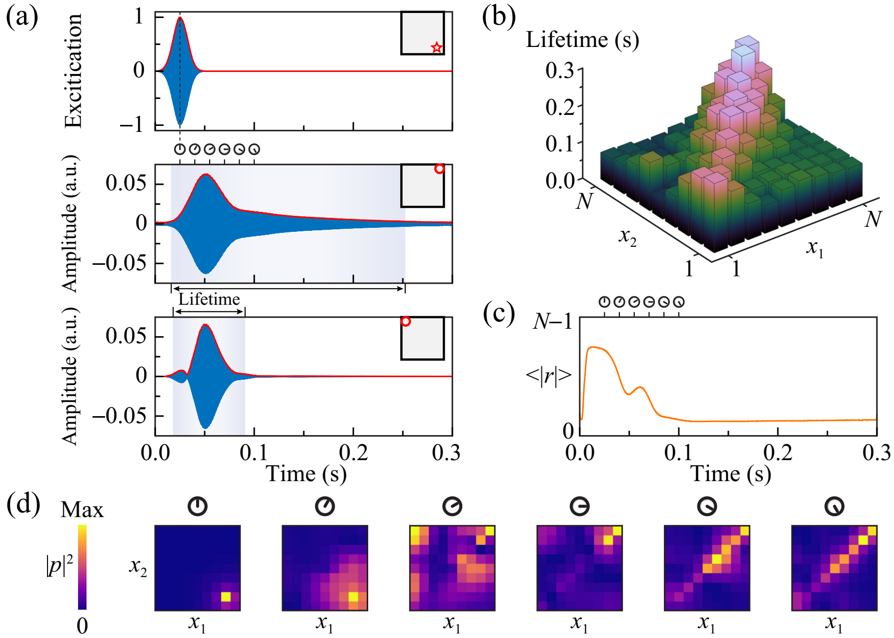

FIG. 4. Observation of time cluster effect. (a) Measurement of the acoustic signals in the time domain. Upper panel: A function of a Gaussian wave packet, launched at the $(x_1, x_2) = (8, 2)$ cavity for excitation. Middle and lower panels: acoustic signals measured at different corner cavities. The excited or measured cavities are marked in the insets. The red curves sketch out the envelope of signals. (b) Lifetimes of the acoustic signal in every cavity. (c) Time evolution of measured $\langle|r|\rangle$. (d) Snapshots of the acoustic field (modulus square) at discretized times, as labeled by the clock markers. Each panel is normalized to its maximum.

transformed into the onsite energies of the diagonal sites (red spheres). The nonreciprocal two-body hoppings are embodied in the hoppings $t_{1,2} = \rho e^{\mp\gamma}$ (blue and red arrows) along the diagonal line.

Developed from Fig. 3(a), the PC sample comprises 9×9 cuboid cavities ($N = 9$), which are filled with air and arranged with 40-mm spacing, as illustrated in Fig. 3(b). The dipole resonance mode of the cavity plays the role of lattice site with a center frequency f_0. The connecting tubes (gray) introduce t_0. Along the diagonal line, nonreciprocal hoppings are accomplished by a set of cross-linked tubes (blue) and custom-made detector-controller-speaker devices, that is, the AECs. The AEC provides unidirectional and tunable acoustic coupling through the holes (red circles) drilled on diagonal cavities, thus bringing nonreciprocity. In addition, the cross-linked tubes would inevitably shift the center frequency of the diagonal sites to $f_0 + U$ and equivalently introduce the onsite two-body interaction term.

To investigate the NHSE and NHISE of acoustic bound pairs, we adopt two AEC setups, as sketched by Figs. 3(c) and 3(d), to attain distinct nonreciprocal hopping strengths $t_{1,2}$ within the same PC sample, and all the acoustic parameters are retrieved from a pre-experiment [32,33]. For the first setup in Fig. 3(c) with $t_1 = \kappa_0$ and $t_2 = \kappa_0 + \kappa_a$, the complex frequency spectrum is computed in Fig. 3(e). The solid lines represent the center-of-mass spectrum under PBC. While the scattering states (black) are confined to a line, the acoustic bound pair state (magenta) winds clockwise along the arrows, corresponding to $v = -1$. This spectral topology implies the accumulation of OBC eigenstates (dots) in the NHSE. Experimentally, we insert a broadband speaker into the center cavity to excite the acoustic bound pair states, and measure the frequency response in each cavity. Figure 3(f) depicts the acoustic field distribution at 3122 Hz, which is the response peak frequency at the upper right corner site and also corresponds to the bound pair states in Fig. 3(e). As expected, the NHSE of bound pair is distinctly visible that, the acoustic signal unidirectionally propagates along the dominant hopping direction (dashed arrow) while preserving its strong localization at the diagonal line.

For the AEC setup in Fig. 3(d), the hopping strengths are decreased as $t_1 = \kappa_0 - \kappa_a$ and $t_2 = \kappa_0$ while the dominant hopping direction remains unchanged. Consequently, the center-of-mass spectrum in Fig. 3(g) exhibits an anticlockwise winding of the acoustic bound pair band, corresponding to a $v = 1$ and implying the reversal of collapse direction under OBC. By performing the same experimental procedure, the NHISE of the acoustic bound pair is demonstrated in Fig. 3(h). At 3150 Hz, the acoustic propagation along the dominant hopping direction almost vanishes while that along the opposite direction is pronouncedly amplified. See more data in Supplemental Material [32].

Time cluster effect—Under nonreciprocal two-body interactions, the time cluster effect is investigated in time-domain measurements of acoustic pulse response.

The input signal has a center frequency of 3122 Hz and the amplitude envelope takes the form of a Gaussian function, as plotted in the upper panel of Fig. 4(a). The red line highlights the envelope curve of the wave packet, which is centered at $t = 0.025$ s (the first clock marker) in the time domain. With the AEC setup in Fig. 3(f), we launch the input signal at the $(x_1, x_2) = (8, 2)$ cavity of the PC to reproduce an initial state of separated particles, and their time evolution is detectable via response signal measurement. The middle and lower panels of Fig. 4(a) exemplify two representative response signals, measured at the corner sites on the diagonal and anti-diagonal lines, respectively. A pronounced divergence emerges: the diagonal cavity exists in a long-lasting wave packet, while in sharp contrast, the signal at the antidiagonal cavity undergoes rapid attenuation. To visualize this divergence, we define the lifetime of the response signal as the lasting time that the envelope curve exceeds 0.003 a.u., as labeled by the shaded regions in Fig. 4(a). More visually, lifetimes for all the cavities are displayed in Fig. 4(b). Compared with those cavities corresponding to scattering states, the diagonal cavities exhibit significantly longer lifetimes, owing to the acoustic bound pair states with larger imaginary parts of eigenfrequencies.

As a matter of fact, the highly contrasting lifetimes give rise to the time cluster effect. We calculate the time evolution of $\langle |r| \rangle$ in Fig. 4(c) based on the measured acoustic signals. Following the launch of the input signal (the first clock marker), the curve of $\langle |r| \rangle$ experiences a sharp decay to zero, unambiguously evidencing the time cluster effect. Furthermore, evolution of the acoustic signal is presented in Fig. 4(d), and the clock markers denote discretized times starting from $t = 0.025$ s and with increments of 0.015 s. In the first three panels, the acoustic signal propagates throughout the PC. Subsequently, owing to the longer lifetime of bound pair states, the signal rapidly distributes along the diagonal line, implying the clustering of particles. The experimental data are in excellent agreement with the theoretical prediction.

Conclusion—In conclusion, we have experimentally investigated the dynamics of correlated bosons under nonreciprocal two-body interactions, using a mapping to the propagation of acoustic waves in a specially designed PC simulator. The resulting NHSE and NHISE of acoustic bound pairs, as well as the time cluster effect, have been adequately addressed in airborne sound measurements. This approach opens new avenues for exploring non-Hermitian phenomena in correlated systems, broadening the insight to many-body physics.

Acknowledgments—We thank Rui Wang and Zhengwei Zuo for helpful discussions at an early stage of this work. This work is supported by the National Key R&D Program of China (No. 2022YFA1404900, No. 2022YFA1404500, and No. 2023YFB2804701), National Natural Science Foundation of China (No. 12374409, No. 12504250, No. 12574024, No. 12574484, and No. U25D8001), Hubei Provincial Natural Science Foundation of China (No. 2025AFB051), China Postdoctoral Science Foundation (No. 2024M752453), and Postdoctoral Fellowship Program of CPSF (No. GZB20240575).

Data availability—The data that support the findings of this article are not publicly available. The data are available from the authors upon reasonable request.

[1] X.-G. Wen, Choreographed entanglement dances: Topological states of quantum matter, Science **363**, eaal3099 (2019).

[2] K. I. Bolotin, F. Ghahari, M. D. Shulman, H. L. Stormer, and P. Kim, Observation of the fractional quantum Hall effect in graphene, Nature (London) **462**, 196 (2009).

[3] Z. Lu, T. Han, Y. Yao, A. P. Reddy, J. Yang, J. Seo, K. Watanabe, T. Taniguchi, L. Fu, and L. Ju, Fractional quantum anomalous Hall effect in multilayer graphene, Nature (London) **626**, 759 (2024).

[4] L. Balents, Spin liquids in frustrated magnets, Nature (London) **464**, 199 (2010).

[5] C. Broholm, R. J. Cava, S. A. Kivelson, D. G. Nocera, M. R. Norman, and T. Senthil, Quantum spin liquids, Science **367**, 263 (2020).

[6] C. H. Greene, P. Giannakeas, and J. Pérez-Ríos, Universal few-body physics and cluster formation, Rev. Mod. Phys. **89**, 035006 (2017).

[7] D. Blume, Few-body physics with ultracold atomic and molecular systems in traps, Rep. Prog. Phys. **75**, 046401 (2012).

[8] S. E. Pollack, D. Dries, and R. G. Hulet, Universality in three- and four-body bound states of ultracold atoms, Science **326**, 1683 (2009).

[9] K. Winkler, G. Thalhammer, F. Lang, R. Grimm, J. Hecker Denschlag, A. J. Daley, A. Kantian, H. P. Büchler, and P. Zoller, Repulsively bound atom pairs in an optical lattice, Nature (London) **441**, 853 (2006).

[10] P. Weckesser, K. Srakaew, T. Blatz, D. Wei, D. Adler, S. Agrawal, A. Bohrdt, I. Bloch, and J. Zeiher, Realization of a Rydberg-dressed extended Bose-Hubbard model, Science **390**, 849 (2025).

[11] Y. Guo, S. Dhar, A. Yang, Z. Chen, H. Yao, M. Horvath, L. Ying, M. Landini, and H.-C. Nägerl, Observation of many-body dynamical localization, Science **389**, 716 (2025).

[12] F. Claro, J. F. Weisz, and S. Curilef, Interaction-induced oscillations in correlated electron transport, Phys. Rev. B **67**, 193101 (2003).

[13] S. Longhi, Photonic Bloch oscillations of correlated particles, Opt. Lett. **36**, 3248 (2011).

[14] G. Corrielli, A. Crespi, G. Della Valle, S. Longhi, and R. Osellame, Fractional Bloch oscillations in photonic lattices, Nat. Commun. **4**, 1555 (2013).

[15] N. A. Olekhno, E. I. Kretov, A. A. Stepanenko, P. A. Ivanova, V. V. Yaroshenko, E. M. Puhtina, D. S. Filonov, B. Cappello, L. Matekovits, and M. A. Gorlach, Topological

edge states of interacting photon pairs emulated in a topolectrical circuit, Nat. Commun. **11**, 1436 (2020).
[16] X. Zhou, W. Zhang, H. Sun, and X. Zhang, Observation of flat-band localization and topological edge states induced by effective strong interactions in electrical circuit networks, Phys. Rev. B **107**, 035152 (2023).
[17] W. Zhang, H. Yuan, H. Wang, F. Di, N. Sun, X. Zheng, H. Sun, and X. Zhang, Observation of Bloch oscillations dominated by effective anyonic particle statistics, Nat. Commun. **13**, 2392 (2022).
[18] W. Zhang, L. Qian, H. Sun, and X. Zhang, Anyonic bound states in the continuum, Commun. Phys. **6**, 139 (2023).
[19] E. J. Bergholtz, J. C. Budich, and F. K. Kunst, Exceptional topology of non-Hermitian systems, Rev. Mod. Phys. **93**, 015005 (2021).
[20] K. Ding, C. Fang, and G. Ma, Non-Hermitian topology and exceptional-point geometries, Nat. Rev. Phys. **4**, 745 (2022).
[21] Y. Ashida, Z. Gong, and M. Ueda, Non-Hermitian physics, Adv. Phys. **69**, 249 (2021).
[22] N. Hatano and D. R. Nelson, Localization transitions in non-Hermitian quantum mechanics, Phys. Rev. Lett. **77**, 570 (1996).
[23] A. Rai, C. Lee, C. Noh, and D. G. Angelakis, Photonic lattice simulation of dissipation-induced correlations in bosonic systems, Sci. Rep. **5**, 8438 (2015).
[24] C. H. Lee, Many-body topological and skin states without open boundaries, Phys. Rev. B **104**, 195102 (2021).
[25] R. Shen and C. H. Lee, Non-Hermitian skin clusters from strong interactions, Commun. Phys. **5**, 238 (2022).
[26] W. Zhang, F. Di, H. Yuan, H. Wang, X. Zheng, L. He, H. Sun, and X. Zhang, Observation of non-Hermitian aggregation effects induced by strong interactions, Phys. Rev. B **105**, 195131 (2022).
[27] Y. Liu and S. Chen, Fate of two-particle bound states in the continuum in non-Hermitian systems, Phys. Rev. Lett. **133**, 193001 (2024).
[28] L. Zhang, Y. Yang, Y. Ge, Y. J. Guan, Q. Chen, Q. Yan, F. Chen, R. Xi, Y. Li, D. Jia *et al.*, Acoustic non-Hermitian skin effect from twisted winding topology, Nat. Commun. **12**, 6297 (2021).
[29] Q. Zhang, Y. Li, H. Sun, X. Liu, L. Zhao, X. Feng, X. Fan, and C. Qiu, Observation of acoustic non-Hermitian Bloch braids and associated topological phase transitions, Phys. Rev. Lett. **130**, 017201 (2023).
[30] X. Wang, W. Wang, and G. Ma, Extended topological mode in a one-dimensional non-Hermitian acoustic crystal, AAPPS Bull. **33**, 23 (2023).
[31] J.-X. Zhong, P. F. de Castro, T. Lu, J. Kim, M. Oudich, J. Ji, L. Shi, K. Chen, J. Lu, Y. Jing *et al.*, Higher-order skin effect and its observation in an acoustic kagome lattice, Phys. Rev. B **111**, 014314 (2025).
[32] See Supplemental Material at http://link.aps.org/supplemental/10.1103/xr3h-j9pv for more derivation and discussion of the theoretical model, details of the PC sample, extra experimental data, and the Methods, which includes Refs. [28–31,33].
[33] W. Suh, Z. Wang, and S. Fan, Temporal coupled-mode theory and the presence of non-orthogonal modes in lossless multimode cavities, IEEE J. Quantum Electron. **40**, 1511 (2004).
[34] S. Yao, F. Song, and Z. Wang, Non-Hermitian Chern bands, Phys. Rev. Lett. **121**, 136802 (2018).
[35] K. Yokomizo and S. Murakami, Non-Bloch band theory of non-Hermitian systems, Phys. Rev. Lett. **123**, 066404 (2019).
[36] K. Zhang, Z. Yang, and C. Fang, Correspondence between winding numbers and skin modes in non-Hermitian systems, Phys. Rev. Lett. **125**, 126402 (2020).
[37] Z. Yang, K. Zhang, C. Fang, and J. Hu, Non-Hermitian bulk-boundary correspondence and auxiliary generalized brillouin zone theory, Phys. Rev. Lett. **125**, 226402 (2020).
[38] R. Lin, T. Tai, L. Li, and C. H. Lee, Topological non-Hermitian skin effect, Front. Phys. **18**, 53605 (2023).